



## Synthesis and characterization of pure and Cu doped CeO<sub>2</sub> nanoparticles: photocatalytic and antibacterial activities evaluation

Govindarasu Killivalavan<sup>1</sup>, Arthur Charles Prabakar<sup>1</sup>, K. Chandra Babu Naidu<sup>2</sup> , Balaraman Sathyaseelan<sup>3,\*</sup> , Gubendiran Rameshkumar<sup>3</sup>, Dhananjayan Sivakumar<sup>4</sup>, Krishnamoorthy Senthilnathan<sup>5</sup>, Iruson Baskaran<sup>6</sup>, Elayaperumal Manikandan<sup>7</sup>, B. Ramakrishna Rao<sup>8</sup>

<sup>1</sup> Research and Development Center, Bharathiar University, Coimbatore-641046, India

<sup>2</sup> Department of Physics, GITAM Deemed to be University, Bangalore-562163, Karnataka, India

<sup>3</sup> Department of Physics, University College of Engineering Arni, Anna University Chennai, Arni 632326, Tamil Nadu, India.

<sup>4</sup> Department of Physics, Sree Krishna College of Engineering, Unai, Anaicut-632101, Tamilnadu, India.

<sup>5</sup> Photonics Division, School of Advanced Sciences, VIT University, Vellore, 632014, Tamil Nadu, India

<sup>6</sup> Department of Physics Arignar Anna Government Arts College, Cheyyar 604407, Tamil Nadu, India

<sup>7</sup> Department of Physics, Thiruvalluvar University College of Arts and Science, Thennangur Village, Vandavasi Taluk, Tiruvannamalai District 604408, India

<sup>8</sup> Department of Chemistry, GITAM Deemed to be University, Bangalore-562163, Karnataka, India

\*corresponding author e-mail address: [bsseelan03@gmail.com](mailto:bsseelan03@gmail.com) | Scopus ID [35734996700](https://orcid.org/0000-0001-9135-4996)

### ABSTRACT

This article reports the effect of pure CeO<sub>2</sub> and Cu (1%, 3% and 5 mol %) doped CeO<sub>2</sub> Nanoparticles (NPs) have been prepared by very simple and improved co-precipitation method. Synthesized NPs has been subjected to several analytical methods, viz. XRD, TEM and UV-Vis spectral analysis. XRD data analysis confirmed that face cubic structure and average size are found to be in the range 5-10nm. Particle size and morphological studies as observed from TEM exhibits almost identical cubical shaped particles with average size 5-8nm. The tuning of band gap energy has been observed from UV-Visible absorption spectrum of cerium oxide NPs upon Cu (1%, 3%, and 5mol %) incorporation. Degradation of the methylene blue (MB) through photocatalysis has been observed for pure and Cu (1%, 3% and 5 mol%) CeO<sub>2</sub> nanoparticles under solar spectrum. In addition, pure and Cu (1%, 3% and 5 mol %) cerium oxide nanoparticles has also been subjected to antibacterial response using different strains.

**Keywords:** *Nanocrystalline Materials, Structural, Co-Precipitation, XRD, SEM, HRTEM, Antibacterial Activity.*

### 1. INTRODUCTION

Most of the organic pollutants discharged from textiles industry are toxic and non-biodegradable by ecological process in nature and it's greatly contaminates water and make environment pollutions. Water is precious natural resources on the earth and it has been polluted mainly by contaminated waste water without proper purification from the textile industry [1, 2].

Oxide semiconductor based photocatalysts shown great potential for effective degradation of organic compounds causing water pollution. The photocatalytic activity of oxide semiconductor can be tuned by controlling and reducing recombination of charge carriers. Metal oxide like TiO<sub>2</sub>, ZnO<sub>2</sub>, SnO<sub>2</sub>, and Fe<sub>2</sub>O<sub>3</sub> are widely studied in the various field of waste water purification fields. CeO<sub>2</sub> is capable of existing in different oxidation states consequent to its oxygen release/supply. In photocatalysis, CeO<sub>2</sub> has drawn considerable attraction due to its outstanding photochemical stable, non-toxicity and economically low. Besides, CeO<sub>2</sub> reveals strong optical spectrum in the UV-visible region that is comparable to TiO<sub>2</sub> photocatalysts. Hence, Cerium oxide nanoparticle is likely to be the most appropriate alternative candidate to TiO<sub>2</sub> since energy band gap of CeO<sub>2</sub> is moreover similar to TiO<sub>2</sub> (3.2 eV) [3, 4]. Nanostructured CeO<sub>2</sub> is a rare earth oxide that has been identified in the purification of waste water due to the large band gap (~3.5 eV) when compared with other metal oxides. The nanosized CeO<sub>2</sub> particles exhibit like large surface area, average particle size, microstructural and scrap

the large solar absorption spectrum and electron-hole pair recombination is one of the key factors that enhance the photocatalytic activity process is due to rapid charge recombination contributes to low efficiency [5, 6].

Metal ions doped cerium oxide has been considered an effective approach to modify physical and chemical properties especially copper (Cu<sup>2+</sup>) ion has an incomplete d orbit level is capable metal to produce large number of electron and having the ability to retard photo-generated charges. Cu<sup>2+</sup> ionic radius is comparable with Ce<sup>3+</sup> (or) Ce<sup>4+</sup> ions, so the doping level of Cu<sup>2+</sup> in cerium oxide can be easily controlled. Doping of copper ion into cerium oxide induces more oxygen vacancies and it improves the photocatalytic activity. Several chemical routes such as co-precipitation [7], hydrothermal technique [8], sol-gel [9], electrodeposition [10], etc., have been used to synthesis the cerium oxide nanoparticles.

Among those techniques we have chosen co-precipitation technique because of low cost, easy to scale up and ecofriendly. In this work, metal ion (Cu) at various concentrations (1mol%, 3mol% and 5mol%) doped cerium oxide NPs synthesized by co-precipitation method and their influence on their structural, morphology, photocatalytic activity and antimicrobial properties against some bacteria species were investigated.

## 2. MATERIALS AND METHODS

Cerium oxide ultrafine particles were prepared through simple precipitation method which comprises sequential steps of (i) mixing, (ii) stirring and (iii) drying. An aqueous solution of Ce(NO<sub>3</sub>)<sub>3</sub>•6H<sub>2</sub>O has been initially prepared. Then, a few drops solution of NaOH and polyethylene glycol (PEG) was added to the base and its pH is maintained at 11. The solution was stirred well until precipitation occurs. The precipitates were washed, dried and the resulting mixture is heated up to a temperature of 110°C for 24 h.

Cu-doped CeO<sub>2</sub> nanoparticles were prepared in three compositions via 1, 3 and 5 mol% by dissolving Cerium nitrate hexahydrate and copper nitrate trihydrate in de-ionized water and the resulting mixture got stirred by adding a few drops of solution of NaOH and PEG till the occurrence of precipitation. The above process was carried out at room temperature and the pH value was maintained at 11. Figure 1. depicts the reaction mechanism in flow chart scheme. The resultant precipitates were washed, dried and heated to temperature of 110° C for 12 h. The final product has been taken for analysis through XRD, SEM and TEM in detail.

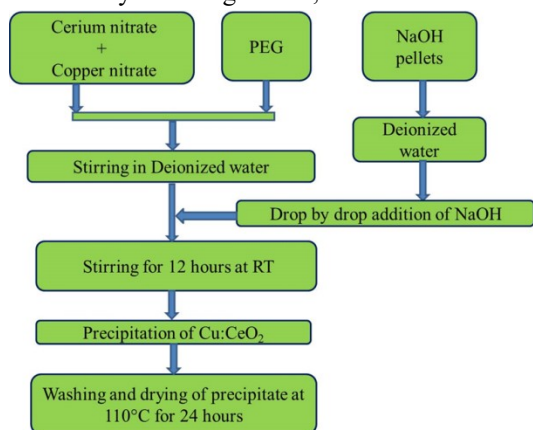


**Figure 1.** Flowchart for synthesis process pure and Cu-doped CeO<sub>2</sub> NPs using Co-precipitation technique.

## 3. RESULTS

### 3.1. X-ray diffraction pattern of CeO<sub>2</sub> and Cu:CeO<sub>2</sub> nanoparticles.

Unit cell property and purity of crystalline phase of CeO<sub>2</sub> and Cu doped (1%, 3% and 5%) cerium oxide nanoparticles have been recorded from PXRD and the pattern is depicted in Fig.2. From the Fig.2, strong peaks in the patterns were corresponds to (111), (220), (200), (222) and (311) (hkl) planes respectively. The results show the FCC unit cell of CeO<sub>2</sub> (JCPDS reference number: 34-0394). There are no peaks corresponding to Cu related impurity phase were detected and it suggests that Cu has entered into CeO<sub>2</sub> matrix. The mean size of pure and Copper doped nanoparticles was computed from XRD diffraction peak corresponds to (111) plane using Scherrer approach is given in equation (1).

$$D = 0.89\lambda / \beta \cos\theta \text{ ----- (1)}$$

Here,  $\beta$  is termed as FWHM (full- width at half maximum) and  $\theta$  represents the angle of diffraction. Average size of CeO<sub>2</sub> and copper doped (1%, 3% and 5%) Cerium oxide nanoparticles were found to be ~10nm, ~8nm, ~7nm and ~5nm respectively. It

### 2.1. Characterization of virgin and Cu-doped CeO<sub>2</sub> nanoparticles.

Powder X-ray diffraction was recorded in the 2 $\theta$  region 15-80° (Bruker, D8 Diffractometer) at a scan rate 2°/min with the aid of Cu-K $\alpha$ 1 source. Scherrer approach was adopted to estimate the average size of the CeO<sub>2</sub> crystallites. Topographical images have been recorded using SEM analysis and from EDX measurements, composition of individual elements was also assessed using Carl Zeiss SUPRA-555 scanning electron microscope. In order to ascertain the results obtained from SEM, Transmission electron microscope has also been studied using PHILIPS, Model: CM200 TEM. Spectral absorption properties of CeO<sub>2</sub> have been studied in the wavelength range 200-800 nm from Shimadzu UV-1800 UV-Vis spectrophotometer.

### 2.2. Antipathogens property study using CeO<sub>2</sub>.

Possible antipathogenic properties of CeO<sub>2</sub> and Cu-doped CeO<sub>2</sub> nanoparticles were experimented using different pathogenic (bacterial) strains. The under mentioned strains of bacteria viz., *S. aureus*, *vancomycin-resistant Enterococcus faecium*, *S.pyogenes*, *E. coli*, *K.pneumonia*, *P.aeruginosa*, *A.baumannii* and *Proteus mirabilis* were commercially produced through American type culture collection and those were actually utilized under well diffusion method.

Synthesised pure CeO<sub>2</sub> and Cu-doped (1%, 3% and 5 mol%) CeO<sub>2</sub> nanoparticles were taken in doubly de ionized water and sonicated. The strain named; *S. aureus*, *vancomycin-resistant Enterococcus faecium*, *S.pyogenes*, *E. coli*, *K.pneumonia*, *P.aeruginosa*, *A.baumannii* and *Proteus mirabilis* were cultured in nutrient broth for 24h at 37°C. Bacterial lawns were prepared using 100 $\mu$ l of nutrient broth culture. In each plate, the wells have been fed with 100 $\mu$ l of our studied powder of CeO<sub>2</sub> and Cu-doped CeO<sub>2</sub>. The observation of microbial inhibition zone in the wells was confirmed after sufficient inhibition period.

revealed that the average size of cerium oxide decreases after Cu doping CeO<sub>2</sub> samples, respectively. The amount of dopant (Cu %) increases the width of the diffraction peak increases, suggesting the quality of crystalline decreases. The average crystallite size and lattice parameters of the pure and Cu doped CeO<sub>2</sub> nanoparticle are given in table 1.

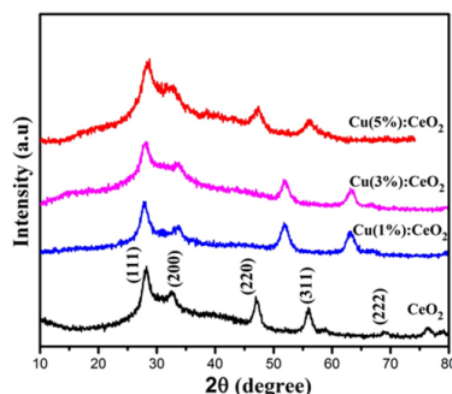


**Figure 2.** PXRD patterns of CeO<sub>2</sub> and Cu:CeO<sub>2</sub> nanoparticles.

### 3.2. SEM and EDX analyse on CeO<sub>2</sub> and Cu:CeO<sub>2</sub> nanoparticles.

SEM images of CeO<sub>2</sub> and Cu- doped CeO<sub>2</sub> nanoparticle are shown in figures 3(a-d). It can be observed that the obtained nanoparticles were highly aggregated in character. For 1 mol% of Cu doping more agglomeration was noticed. This confirms the reduction in crystalline size significantly by adding Cu ions to CeO<sub>2</sub> host. The quantitative elemental analysis was performed using EDAX. The observed EDAX spectrum of Pure and Cu doped CeO<sub>2</sub> was shown in figure 4 (a-d). From the spectrum it can be seen that the cerium and copper absorption were strongly observed, which confirms the stoichiometric concentration of the elements.

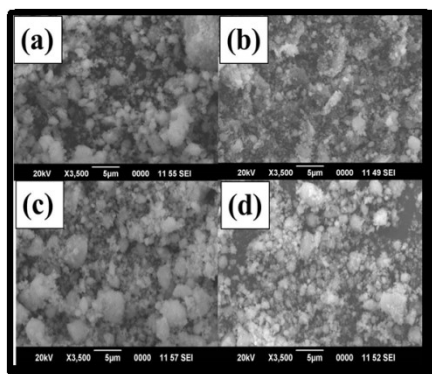
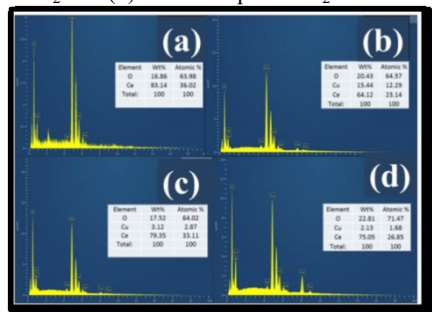


**Figure 3.** SEM micrographs of (a) pure CeO<sub>2</sub> (b) 1% Cu doped CeO<sub>2</sub> (c) 3% Cu doped CeO<sub>2</sub> and (d) 5% Cu doped CeO<sub>2</sub> NPs with magnification.



Element	Wt%	Atomic %
O	16.86	63.98
Ce	83.14	36.02
Total:	100	100

**Figure 4.** EDAX spectra of (a) CeO<sub>2</sub> (b) Cu (1%) doped CeO<sub>2</sub> (c) Cu (3%) doped CeO<sub>2</sub> and (d) Cu (5%) :CeO<sub>2</sub> nanoparticles.

### 3.3. Transmission Electron Microscopy (TEM) analysis on CeO<sub>2</sub> and Cu doped CeO<sub>2</sub> nanoparticles.

TEM with SAED analysis on CeO<sub>2</sub> and Cu:CeO<sub>2</sub> at various concentrations of Cu shows that the majority of the particles are having size nearly at 10 nm and it can be ascertained from particle size histogram shown in Fig.5. Strikingly, an increase in doping decrease the particle sizes and it is shown in figure 4. This result appears to be consonating with XRD. SAED further substantiation

the cubical phase of CeO<sub>2</sub> and its phase groups agree with earlier reports [11, 12].

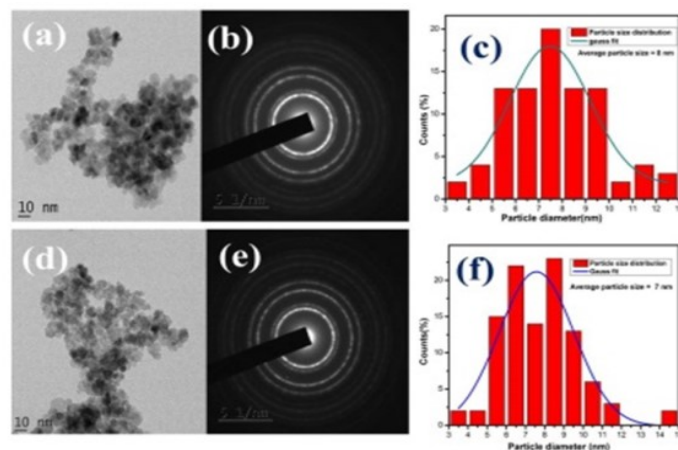


**Figure 5.** TEM micrographs of (a) CeO<sub>2</sub> (d) Cu 3% doped CeO<sub>2</sub> (b) SAED patterns of pure CeO<sub>2</sub> (e) Cu 3% doped CeO<sub>2</sub> and (c) distribution of particle size histogram of pure CeO<sub>2</sub> (f) Cu (3%) doped CeO<sub>2</sub> NPs with magnification.

### 3.4. Optical absorption measurements on Cu-doped Cerium oxide nanoparticles.

In order to confirm the optical property and substitution of Cu into CeO<sub>2</sub> matrix, the doped nanoparticles were analysed by UV-Vis spectrophotometer. UV-Visible spectra of the CeO<sub>2</sub> and Cu doped cerium oxide nanoparticles at various concentration (1mol%, 3mol% and 5mol%) shows that maximum absorption peak was around at 321 nm region and this peak found to have shifted towards longer wavelength region (red shift) upon doping of Cu ion percentage and this is indicated in figure 6 (a). The energy band gap was obtained for CeO<sub>2</sub> from Tauc plot using the following equation (2).

$$ah\nu = A(h\nu - E_g)^n \text{----- (2)}$$

Where,  $h\nu$  is incident energy, 'A' termed as a constant of transition probability and  $n = 0.5$  for direct transition shown in Fig. 6(b). The calculated values for pure CeO<sub>2</sub> are about 2.82 eV and this value got decreased to 2.74, 2.68 and 2.56eV eV for Cu (1%, 3% and 5 mol %) doped samples showing an increase in the absorption in the longer wavelength region. The indirect band gap energy is well in agreement with the literature [13, 14].

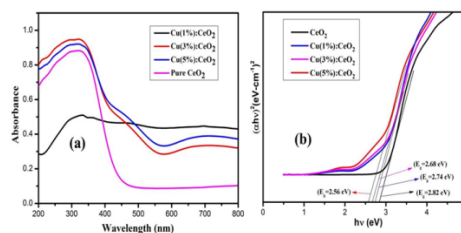


**Figure 6.** (a) UV-Visible absorption spectrum of CeO<sub>2</sub> (b) Tauc plots for pure and Cu doped CeO<sub>2</sub> nanoparticles.

**Table.1.** Crystalline size, lattice parameters of doped CeO<sub>2</sub> nanoparticles at various dopant concentrations.

Sl.No	Name of the compounds	Lattice parameters (Å°)	Interplanar spacing(d) (Å°)	Average Crystalline size (nm)	Nature of strain
1	Cu(1%):CeO <sub>2</sub>	5.470(6)	3.17275	~ 8	Compression
2	Cu(3%):CeO <sub>2</sub>	5.470(2)	3.15825	~ 7	
3	Cu(5%):CeO <sub>2</sub>	5.374(5)	3.10298	~ 5	
1	Cu(1%):CeO <sub>2</sub>	5.470(6)	3.17275	~ 8	
2	Cu(3%):CeO <sub>2</sub>	5.470(2)	3.15825	~ 7	



Sl.No	Name of the compounds	Lattice parameters (Å <sup>o</sup> )	Interplanar spacing(d) (Å <sup>o</sup> )	Average Crystalline size (nm)	Nature of strain
3	Cu(5%):CeO <sub>2</sub>	5.374(5)	3.10298	~ 5	
1	Cu(1%):CeO <sub>2</sub>	5.470(6)	3.17275	~ 8	
2	Cu(3%):CeO <sub>2</sub>	5.470(2)	3.15825	~ 7	
3	Cu(5%):CeO <sub>2</sub>	5.374(5)	3.10298	~ 5	

**Table 2.** Bandgap energy value of pure and copper doped CeO<sub>2</sub> NPs at various dopant concentrations.

Sl.No	Name of the compound	Dopant concentration	E <sub>g</sub> (eV)
1	CeO <sub>2</sub>	-	2.82
2	CeO <sub>2</sub>	1%	2.74
3	CeO <sub>2</sub>	3%	2.68
4	CeO <sub>2</sub>	5%	2.56

### 3.5. Photocatalytic dye degradation activity of Cu-CeO<sub>2</sub> nanoparticles.

Solar radiation in the wavelength region of 4000-7000 Å used as the light source. In this procedure 10 mg of the pure cerium oxide powder was dissolved in 10 mL solution of MB (10mg/L). The reaction stirred for 2 hours under the dark condition to achieve adsorption equilibrium before the illumination of light then the solution of MB with photocatalyst was analysed by UV-Vis spectroscopy.

The solution was illuminated in the solar spectrum during the day time 10 am to 3 pm at the temperature ranging from 30-33°C under the constant and continuous magnetic stirring. The relative strength of MB in the treated liquid mixture was periodically analysed through optical absorption spectroscopy (UV-Vis-NIR spectrophotometer) at the regular interval time of 1 hour. Pure CeO<sub>2</sub> photocatalyst used as the photocatalytic reference for the comparison with other doped nanoparticles. Photocatalytic properties of Cu doped CeO<sub>2</sub> NPs were analysed decomposition of the MB in the aqueous solution under sunlight. If there is no photocatalyst involved, the MB solution is stable under UV and visible radiation.

In order to evaluate the influence of copper ion in modifying the methylene blue dye degradation properties of copper doped CeO<sub>2</sub> photocatalyst taken for photo degradation activity. From the Fig. 7 (a-d) it's also found that the strong absorption spectra peak located at the wavelength of 647 nm decreases gradually with increases illumination time and absorbance of MB reduced greatly after 5 hours of solar radiation using the copper doped CeO<sub>2</sub> nanoparticles and it shows better photocatalytic activity than pure CeO<sub>2</sub> due to reduction in the bandgap after doping with copper ions.

Pure CeO<sub>2</sub> shows lower photocatalytic activity than doped one due to more and fast recombination of electrons and holes Cu<sup>2+</sup> ion was used to reduce the e-h recombination. The photocatalytic activity has been observed for 1% and 3% Cu doped CeO<sub>2</sub> with degrading MB about 60% while 5% Cu doped CeO<sub>2</sub> was most effective in MB degradation showing 72% at 5 hours. Copper ion acted as electron trap, OH groups on the surface after illumination act as hole trap, sites of adsorption and sources of the OH radicals.

The photocatalytic activity increases with an increase in hydroxyl group on the catalyst surface. Without photocatalyst or without illumination the catalyst shows small degradation of dyes

in the dark, it indicates that the catalyst and light are important for fast photocatalytic dye degradation.

The degradation rate of aquo MB solutions that has 72% under visible irradiation in 5h using Cu 5% doped shows higher photocatalytic activity than pure CeO<sub>2</sub> NPs. and it is projected in Fig. 7 (e).

The chemical kinetic reaction involved during MB degradation has been explained from the Pseudo-first order model. The rate of reaction can be shown shown in equation (3).

$$\ln(C_0/C_t) = Kt \text{ ----- (3)}$$

C<sub>0</sub> and C<sub>t</sub> are the dye concentration at initial and various time. K- Constant of reaction rate at the lower order. It can be calculated from simulation curve as shown in figure 7 (f). R<sup>2</sup> values are tabulated in Table 3. [15, 16].

The efficiency of photocatalytic degradation for pure and doped Cu:CeO<sub>2</sub> NPs were also determined using the following equation

$$\text{Efficiency} = (C_0 - C_t)/C_0 * 100\% \text{ -----(4)}$$

The results are shown in Fig. 7(e) by plotting photocatalytic degradation efficiency vs irradiation time. All the photocatalyst shows the good photocatalytic activity of MB dye degradation in visible light radiation.

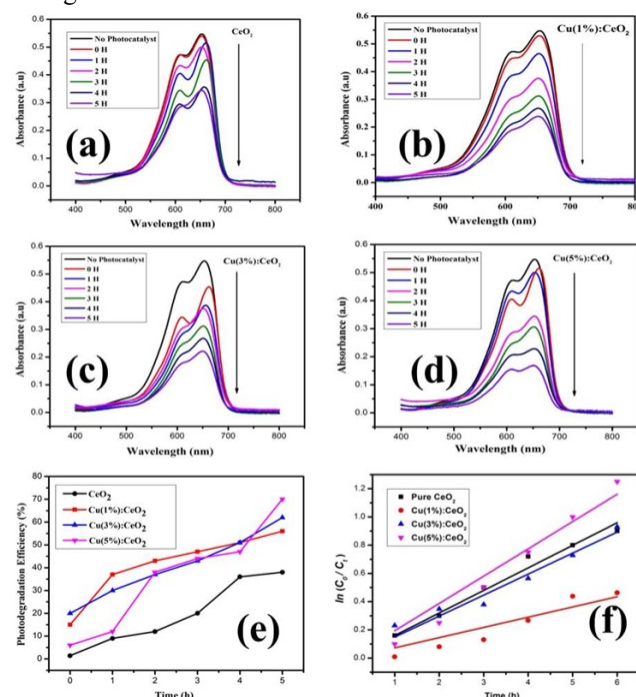


**Figure 7.** Degradation of aqueous MB dye through photocatalysis using (a) CeO<sub>2</sub> (b) 1 mol % Cu: CeO<sub>2</sub> (c) 3mol % Cu:CeO<sub>2</sub> (d) 5mol % Cu:CeO<sub>2</sub> (e) efficiency percentage of degradation at various illumination time (f) Reaction kinetic curves for the photodegradation of nano CeO<sub>2</sub> samples.

### 3.6 Antibacterial activity of Cu Doped CeO<sub>2</sub> NP's

Antibacterial activity of Copper ion doped cerium oxide nanoparticles was investigated using the method described elsewhere [17]. The bacterial strains namely; *S. aureus*, vancomycin-resistant *Enterococcus faecium* (VREF), *S.pyogenes*,

*E. coli*, *K.pneumoniae*, *P.aeruginosa*, *A.baumannii* and *Proteus mirabilis* have been identified as the potential strains for testing. Inhibition zone values of every strain with our material are provided in table 4.

From table 4, it shows that all the doped nanoparticles were found to be affective only against *Acinetobacter baumannii* among other gram negative bacteria, a rare finding at 40 mg concentration inhibited area/diameter extending right from 11mm-16mm. From Fig. 8, the highest diameter of 16mm was formed in 1% copper dopes cerium oxide nanoparticles at concentration of 40 mg, considered to be sensitive.

*Acinetocater baumannii* is the one of the most dangerous bacterium responsible for ventilator associated pneumonia causing 70% nosocomial mortality. It is a need of the hour to reduce infection than treating it [18]. Where 90.38% of the microbes were resistant to one or more aminoglycosides, 76.93% were resistant to fluoroquinolones, 86.54% to trimethoprim-sulphamethoxazole and only 21.15% to tetracycline. It's time to go for toxicity studies in cell lines and animal models and to elucidate the principle for 40 mg concentration of 1% copper doped cerium oxide nanoparticles as antimicrobial substance for controlling the nosocomial infections.

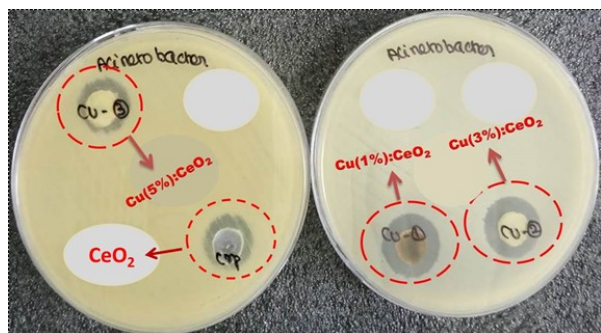


Figure 8. Zone of inhibition of synthesized pure and Cu-doped CeO<sub>2</sub> NPs against various gram negative bacterial pathogens (*A. baumannii*).

Similarly against gram positive clinical isolates *S. aureus*, VREF and *S. pyogenes* only 1% copper doped cerium oxide nanoparticles showed 22mm, 24mm and 11mm as zone of inhibition respectively and it is marked as white circle shown in Fig.9. It indicates that *S. aureus* and Enterococcus were sensitive to 1 mol % copper doped cerium oxide nanoparticles. A steadily increasing proportion of *S. aureus* is becoming resistant to Enterococcus and even newly developed medicines such as dalfopristin/quinopristin and linezolid [19, 20,21,].

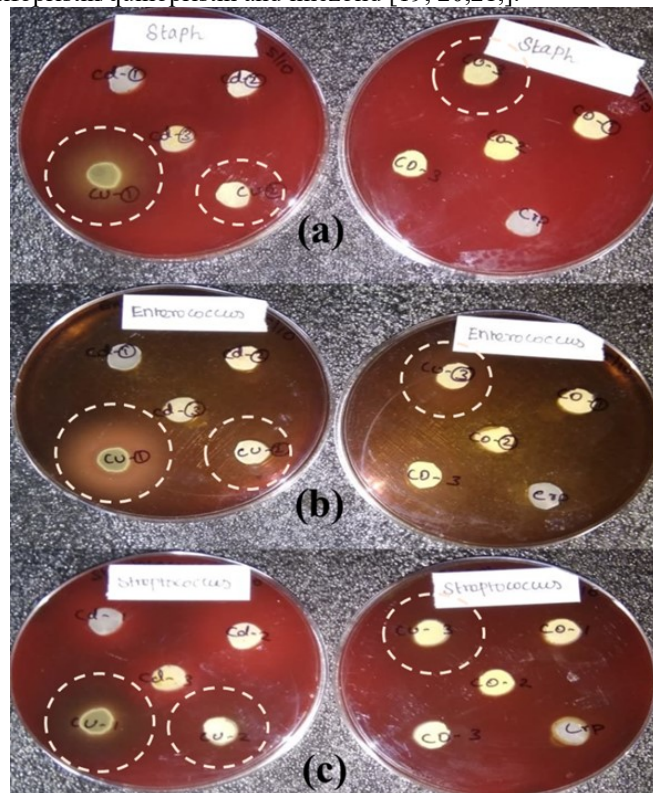


Figure 9. Zone of inhibition of synthesized pure and Cu-doped CeO<sub>2</sub> NPs against various gram positive bacterial pathogens (a) *S. aureus*, (b) *Enterococcus* (c) *S. pyogenes*

Table 3. First order rate constant and R<sup>2</sup> values of CeO<sub>2</sub> and Cd:CeO<sub>2</sub> nanoparticles at different concentrations.

Sl.No	Sample Name	Slope (k)	Standard Error	R value	R <sup>2</sup> value
1	CeO <sub>2</sub>	0.1597	±0.0048	0.99768	0.9946
2	Cu(1%):CeO <sub>2</sub>	0.07243	±0.0071	0.97677	0.9449
3	Cu(3%):CeO <sub>2</sub>	0.14873	±0.006	0.99546	0.9903
4	Cu(5%):CeO <sub>2</sub>	0.19341	±0.00978	0.99366	0.9848

Table 4. antibacterial activity of synthesized pure and Cu-doped CeO<sub>2</sub> nanoparticles against pathogens of both gram negative and gram positive types.

Bacterial Strain		Zone of inhibition (mm)			
		CeO <sub>2</sub>	Cu:CeO <sub>2</sub> (1mol %)	Cu:CeO <sub>2</sub> (3mol %)	Cu:CeO <sub>2</sub> (5mol %)
Gram Positive	<i>S. aureus</i>	-	22	-	-
	VREF	-	24	-	-
	<i>S.pyogenes</i>	-	11	-	-
Gram Negative	<i>E. coli</i>	-	-	-	-
	<i>K.pneumonia</i>	-	-	-	-
	<i>P.aeruginosa</i>	-	-	-	-
	<i>P. mirabilis</i>	-	-	-	-
	<i>A.baumannii</i>	11	16	15	12

#### 4. CONCLUSIONS

We have successfully synthesized pure and Cu doped CeO<sub>2</sub> NPs via the co-precipitation method. Powder XRD pattern ascertains that the cubical unit cell of CeO<sub>2</sub> NPs. Photocatalytic dye degradation efficiencies on synthesized nanoparticle viz., pure CeO<sub>2</sub> and Cu doped (1%, 3% and 5%) CeO<sub>2</sub> has been assessed

using methylene blue dye at various illumination periods of solar light. The degradation efficiencies the chosen photocatalysts are 36% and 38%, 62% and 72% respectively for pure CeO<sub>2</sub> and Cu doped (1%, 3% and 5%) CeO<sub>2</sub> systems. Based on the performance of the antibacterial activity, 1mol% Cu doped cerium oxide NPs



showed the maximum inhibition zone against pathogenic bacteria species. It was found that Cu: CeO<sub>2</sub> doped at 1% has the highest level of antimicrobial properties against both for Gram positive

(*S. aureus*, *Enterococcus* and *S.pyogenes*) and Gram negative (*A.baumannii*).

## 5. REFERENCES

1. Khan, S.B.; Faisal, M.; Rahman, M.M.; Jamal, A. Exploration of CeO<sub>2</sub> nanoparticles as a chemi-sensor and photo-catalyst for environmental applications. *Science of the Total Environment* **2011**, *409*, 2987-2992, <https://doi.org/10.1016/j.scitotenv.2011.04.019>.
2. Sirianuntapiboon, S.; Srisornsak, P. Removal of disperse dyes from textile wastewater using bio-sludge. *Bioresource Technology* **2007**, *98*, 1057-1066, <https://doi.org/10.1016/j.biortech.2006.04.026>.
3. Faisal, M.; Khan, S.B.; Rahman, M.M.; Jamal, A.; Akhtar, K.; Abdullah, M.M. Role of ZnO-CeO<sub>2</sub> nanostructures as a photo-catalyst and chemi-sensor. *Journal of Materials Science & Technology* **2011**, *27*, 594-600, [https://doi.org/10.1016/s1005-0302\(11\)60113-8](https://doi.org/10.1016/s1005-0302(11)60113-8).
4. Khan, S.B.; Faisal, M.; Rahman, M.M.; Akhtar, K.; Asiri, A.M.; Khan, A.; Alamry, K.A. Effect of surfactant on the particle size, photocatalytic activity and sensing properties of CeO<sub>2</sub> nanoparticles. *International Journal of Electrochemical Sciences* **2013**, *8*, 7284-7297.
5. Primo, A.; Marino, T.; Corma, A.; Molinari, R.; García, H. Efficient visible light photocatalytic water splitting by minute amounts of gold supported on nanoparticulate CeO<sub>2</sub> obtained by a biopolymer templating method. *Journal of American Chemical Society* **2011**, *133*, 6930-6933, <https://doi.org/10.1021/ja2011498>.
6. Ravishankar, T.N.; Ramakrishna, T.; Nagaraju, G.; Rajanaika, H. Synthesis and characterization of CeO<sub>2</sub> nanoparticles via solution combustion method for photocatalytic and antibacterial activity studies. *Chemistry Open* **2015**, *4*, 146-154, <https://doi.org/10.1002/open.201402046>.
7. Shih, C. J.; Chen, Y.J.; Hon, M. H. Synthesis and crystal kinetics of cerium oxide nanocrystallites prepared by co-precipitation process. *Materials Chemistry and Physics* **2010**, *121*, 99-102, <https://doi.org/10.1016/j.matchemphys.2010.01.001>.
8. Zhou, Y.C.; and Rahaman, M.N. Hydrothermal synthesis and sintering of ultrafine CeO<sub>2</sub> powders *Journal of Materials Research* **1993**, *8*, 1680-1686, <https://doi.org/10.1557/jmr.1993.1680>.
9. Li, L.P.; Lin, X.M.; Li, G.S.; Inomata, H. Solid solubility and transport properties of Ce<sub>1-x</sub>Nd<sub>x</sub>O<sub>2-δ</sub> nanocrystalline solid solutions by a sol-gel route. *Journal of Materials Research* **2001**, *16*, 3207-3213, <https://doi.org/10.1557/jmr.2001.0442>.
10. Yang, L.; Pang, X.; Fox-Rabinovich, G.; Veldhuis, S.; Zhitomirsky, I. Electrodeposition of cerium oxide films and composites. *Surfacing and Coating Technology* **2011**, *206*, 1-7, <https://doi.org/10.1016/j.surfcoat.2011.06.029>.
11. Kaviyarasu, K.; Manikandan, E.; Nuru, Z.Y.; Maaza, M. Investigation on the structural properties of CeO<sub>2</sub> nanofibers via CTAB surfactant. *Materials Letters* **2015**, *160*, 61-63, <https://doi.org/10.1016/j.matlet.2015.07.099>.
12. Xue, L.; He, H.; Liu, C.; Zhang, C.; Zhang, B. Promotion Effects and Mechanism of Alkali Metals and Alkaline Earth

- Metals on Cobalt-Cerium Composite Oxide Catalysts for N<sub>2</sub>O Decomposition. *Environmental Science & Technology* **2009**, *43*, 890-895, <https://doi.org/10.1021/es801867y>.
13. Zhang, H.; He, X.; Zhang, Z.; Zhang, P.; Li, Y.; Ma, Y.; Kuang, Y.; Zhao, Y.; Chai, Z. Nano-CeO<sub>2</sub> Exhibits Adverse Effects at Environmental Relevant Concentrations. *Environmental Science & Technology* **2011**, *45*, 3725-3730, <https://doi.org/10.1021/es103309n>.
14. Zhang, Q.C.; Yu, Z.H.; Li, G.; Ye, Q.M.; Lin, J.H. Synthesis of quantum-size cerium oxide nanocrystallites by a novel homogeneous precipitation method. *Journal of Alloys and Compounds* **2009**, *477*, 81-84, <https://doi.org/10.1016/j.jallcom.2008.10.059>.
15. Saravanakumar, K.; Ramjan, M.M.; Suresh, P.; Muthuraj, V. Fabrication of highly efficient visible light driven Ag/CeO<sub>2</sub> photocatalyst for degradation of organic pollutants. *Alloys and Compounds* **2016**, *664*, 149-160, <https://doi.org/10.1016/j.jallcom.2015.12.245>.
16. Zhang, L.; Zhang, Q.; Xie, H.; Guo, J.; Lyu, H.; Li, Y.; Sun, Z.; Wang, H.; Guo, Z. Electrospun titania nanofibers segregated by graphene oxide for improved visible light photocatalysis. *Applied Catalysis B: Environmental* **2017**, *201*, 470-478, <https://doi.org/10.1016/j.apcatb.2016.08.056>.
17. Sirelkhatim, A.; Mahmud, S.; Seeni, A.; Mohamad Kaus, N.H.; Ann, L.C.; Bakhori, S.K.M.; Hasan, H.; Mohamad, D. Review on Zinc Oxide Nanoparticles: Antibacterial Activity and Toxicity Mechanism. *Nano-Micro Letters* **2015**, *7*, 219-242, <https://doi.org/10.1007/s40820-015-0040-x>.
18. Peleg, A.Y.; Seifert, H.; Paterson, D.L. *Acinetobacter baumannii*: Emergence of a Successful Pathogen. *Clinical Microbiology Reviews* **2008**, *21*, 538-582, <https://doi.org/10.1128/cmr.00058-07>.
19. Castillo, N.R.; Frisanch, J.A.; Rinsky, J.L.; Resnick, C.; Carroll, K.C.; Rule, A.M.; Silbergeld, E.K. Multidrug-Resistant and Methicillin-Resistant *Staphylococcus aureus* (MRSA) in Hog Slaughter and Processing Plant Workers and Their Community in North Carolina (USA). *Environmental Health Perspectives* **2014**, *122*, 471-477, <https://doi.org/10.1289/ehp.1306741>.
20. Pourhajibagher, M.; Chiniforush, N.; Bahador, A. Antimicrobial action of photoactivated C-Phycocyanin against *Enterococcus faecalis* biofilms: Attenuation of quorum-sensing system. *Photodiagnosis and Photodynamic Therapy* **2019**, *28*, 286-291, <https://doi.org/10.1016/j.pdpdt.2019.10.013>.
21. Sivakumar, D, Chandra Babu Naidu, K, Prem Nazeer.K., Mohamed Rafi.M, Ramesh kumar.G, Sathyaseelan.B, Killivalavan.G, Ayisha Begam.A Structural Characterization and Dielectric Studies of Superparamagnetic Iron Oxide Nanoparticles. *Journal of the Korean Ceramic Society* **2018**, *55*(3), 230-238, <https://doi.org/10.4191/kcers.2018.55.3.02>.

